Ultrasound in Medicine & Biology 000 (2023) 1–6

Contents lists available at ScienceDirect

Ultrasound in Medicine & Biology

journal homepage: www.elsevier.com/locate/ultrasmedbio

Original Contribution

Effect of Anesthetic Carrier Gas on *In Vivo* Circulation Times of Intravenously Administered Phospholipid Oxygen Microbubbles in Rats

Phillip G. Durham [a,b], Awaneesh Upadhyay [c], J. Angel Navarro-Becerra [c], Richard E. Moon [d], Mark A. Borden [c], Paul A. Dayton [a,b], Virginie Papadopoulou [b,*]

[a] *Eshelman School of Pharmacy, University of North Carolina, Chapel Hill, NC, USA*
[b] *Joint Department of Biomedical Engineering, University of North Carolina and North Carolina State University, Chapel Hill, NC, USA*
[c] *Department of Mechanical Engineering, University of Colorado, Boulder, CO, USA*
[d] *Departments of Anesthesiology and Medicine, Center for Hyperbaric Medicine and Environmental Physiology, Duke University, NC, USA*

ARTICLE INFO

Keywords:
Bubble
Contrast-enhanced ultrasound
Ultrasound contrast agent
Tumor hypoxia
Radiation therapy

Objective: For the treatment of tumor hypoxia, microbubbles comprising oxygen as a majority component of the gas core with a stabilizing shell may be used to deliver and release oxygen locally at the tumor site through ultrasound destruction. Previous work has revealed differences in circulation half-life *in vivo* for perfluorocarbon-filled microbubbles, typically used as ultrasound imaging contrast agents, as a function of anesthetic carrier gas. These differences in circulation time *in vivo* were likely due to gas diffusion as a function of anesthetic carrier gas, among other variables. This work has motivated studies to evaluate the effect of anesthetic carrier gas on oxygen microbubble circulation dynamics.
Methods: Circulation time for oxygen microbubbles was derived from ultrasound image intensity obtained during longitudinal kidney imaging. Studies were constructed for rats anesthetized on inhaled isoflurane with either pure oxygen or medical air as the anesthetic carrier gas.
Results: Results indicated that oxygen microbubbles were highly visible via contrast-specific imaging. Marked signal enhancement and duration differences were observed between animals breathing air and oxygen. Perhaps counterintuitively, oxygen microbubbles disappeared from circulation significantly faster when the animals were breathing pure oxygen compared with medical air. This may be explained by nitrogen counterdiffusion from blood into the bubble, effectively changing the gas composition of the core, as has been observed in perfluorocarbon core microbubbles.
Conclusion: Our findings suggest that the apparent longevity and persistence of oxygen microbubbles in circulation may not be reflective of oxygen delivery when the animal is anesthetized breathing air.

Introduction

Radiation therapy is an effective tool for the treatment of cancer. As in most oncology treatments, however, there are also significant risks associated with radiation therapy. One major mechanism of radiation-induced cell damage is the creation of single- and double-strand breaks in DNA from the impingement of high-energy particles and the generation of reactive oxygen species, often described as the oxygen fixation hypothesis [1–3]. In the presence of sufficient oxygen, the fragmented DNA strands are molecularly fixed, converting to peroxyl radicals that are unable to be repaired by cellular machinery, leading ultimately to cell death. However, in the absence of oxygen, the damaged DNA can be chemically reduced and repaired, resulting in reduction of permanent damage [1,4].

Hypoxia, or the absence of oxygen, is a hallmark feature of solid tumors. Tumor growth may outpace new vessel formation, increases in interstitial pressure may collapse existing vasculature and increased metabolic activity can further deplete available oxygen in tissue. Although there are many additional effects of hypoxia on cell regulation and stress tolerance [5,6], the lack of available oxygen greatly reduces radiotherapeutic efficacy in hypoxic cells and tumors [7,8]. It follows that oxygen delivery to tumors prior to or during radiation therapy could improve treatment efficacy. Strategies for tumor oxygenation have been explored, such as hyperbaric oxygen therapy, carbogen breathing and vasodilators [9–11], as well as oxygen delivery via perfluorocarbon emulsions [12,13].

Microbubble ultrasound contrast, consisting of a poorly water-soluble gas stabilized by a shell material, has been used for diagnostic imaging for decades in the clinic. In addition to their diagnostic uses, it has been recognized that microbubbles can be used for therapeutic outcomes, both as delivery vehicles themselves and as an agent to enhance

Abbreviations: OMB, oxygen microbubble(s); DBPC, 1,2-dibehenoyl-sn-glycero-3-phosphocholine; DSPE-PEG2000, 1,2-distearoyl-sn-glycero-3-phosphoethanolamine-N-(polyethylene glycol 2000); PBS, phosphate buffered saline; CPS, Cadence contrast pulse sequence; TIC, time-intensity curve(s); AU, arbitrary unit(s); ROI, region of interest; SEM, standard error of the mean; MIP, maximum intensity projection; MAP, mean arterial pressure; CEUS, contrast-enhanced ultrasound

* Corresponding author. 9004 Mary Ellen Jones Building, 116 Manning Drive, Chapel Hill, NC 27599-7575, USA.
E-mail address: papadopoulou@unc.edu (V. Papadopoulou).

https://doi.org/10.1016/j.ultrasmedbio.2023.04.016
Received 26 January 2023; Revised 22 April 2023; Accepted 26 April 2023

Please cite this article as: P.G. Durham et al., Effect of Anesthetic Carrier Gas on *In Vivo* Circulation Times of Intravenously Administered Phospholipid Oxygen Microbubbles in Rats, Ultrasound in Medicine & Biology (2023), https://doi.org/10.1016/j.ultrasmedbio.2023.04.016

transfer of acoustic energy to tissue. Many parts of the microbubble may be functionalized for the purposes of carrying drug payloads, and their responsiveness to an acoustic field allows them to be destroyed in a specific region, releasing their payload [14]. Microbubbles for imaging are traditionally filled with low-solubility gasses such as sulfur hexafluoride and octafluoropropane to increase their circulation lifetime. However, the core gas can be replaced for the purpose of gas delivery [15,16]. Oxygen-filled microbubbles (OMBs) have been investigated as theranostic agents to reverse oxygen depletion, primarily in the contexts of hypoxemia and tumor radiosensitization. Pre-clinical results in a rabbit model of complete tracheal occlusion have indicated that intraperitoneal infusion of OMBs can significantly prolong survival [17]. The strategy of peritoneal microbubble oxygenation has also had promising results in a rat model of acute respiratory distress syndrome, resulting in a 37% increased survival rate compared with that of untreated and saline-treated control groups [18]. As an adjuvant cancer theranostic agent, OMBs have been found to re-oxygenate tumors and improve sonodynamic therapy, brachytherapy and external beam radiation therapy in rodent models [19–24].

Isoflurane is a common anesthetic used for rodent experiments. Isoflurane is administered with a calibrated vaporizer that volatilizes isoflurane into a carrier gas stream, which is delivered to the animal via nose cone. Inhaled anesthesia carried on oxygen gas is commonly employed for pre-clinical studies in rodents. However, contrast-enhanced ultrasound, as well as radiation therapy, is usually performed with human patients breathing air.

The purpose of this study was to evaluate the effect of anesthetic carrier gas on dissolution and clearance kinetics of intravenously administered oxygen microbubbles. It was initially hypothesized that breathing oxygen as the anesthetic carrier gas would reduce oxygen microbubble dissolution and result in longer circulation kinetics.

Methods

Oxygen microbubble preparation

Oxygen microbubbles were synthesized as described previously [22]. Briefly, 1,2-dibehenoyl-*sn*-glycero-3-phosphocholine (DBPC) and 1,2-distearoyl-*sn*-glycero-3-phosphoethanolamine-*N*-(polyethylene glycol 2000) (DSPE-PEG2000) in a 9:1 mol ratio were dissolved in phosphate-buffered saline (PBS) at a total lipid concentration of 12 mg/mL. Lipid and emulsifier were added to 10 × diluted PBS. The system was heated to the main phase transition temperature of the main lipid (75°C) constituent and stirred gently using a magnetic stir bar to make a homogenous suspension. The heated lipid suspension was further subjected to low-power probe sonication (30% amplitude) for 10 min (Branson Digital Sonifier SFX 550, Danbury, CT, USA) to further disperse multilamellar structures into unilamellar structures. The lipid suspension was then cooled to 4°C.

Oxygen-filled microbubbles were then generated by sonicating the lipid solution (Branson, Danbury, CT, USA) in a water-cooled (5°C) continuous-flow closed chamber, under oxygen atmosphere. Resulting OMBs and foam were collected and processed via differential centrifugation to separate unreacted lipid suspension and macrofoams from the OMB microfoam cake containing OMBs with a volume weighted diameter <10 μm. The OMB microfoam obtained was characterized with respect to final size and concentration, as measured by single-particle optical sizing (AccuSizer 780, NICOMP Particle Sizing Systems, Santa Barbara, CA, USA). OMBs were stored at a high concentration (70% −80% v/v) and diluted to 50% gas fraction in oxygen-saturated PBS immediately prior to administration.

Microbubble time–intensity curves

All animal experiments were reviewed and approved by the University of North Carolina Institutional Animal Care and Use Committee. Healthy female Fisher 344 rats (~125 g) were anesthetized with isoflurane (2.5%) with either pure oxygen or medical air carrier gas and placed on a heated imaging platform in the right lateral recumbent position (Fig. 1). Contrast-naïve animals (n = 6 per group) were used for each acquisition to mitigate any confounding effect of antibody-mediated microbubble clearance, which has been previously observed with repeated administration of lipid-shelled microbubbles decorated with PEG [25]. Animals were shaved and depilated over the left kidney. Ultrasound images of the longitudinal view of the kidney were acquired using Cadence contrast pulse sequence (CPS) at 7 MHz (20 Hz frame rate) with a 15L8 linear array transducer (Acuson Sequoia 512, Siemens Medical Solutions USA, Issaquah, WA, USA) at a mechanical index of 0.18, with 80 dB dynamic range and a CPS gain of 0 with uniform time-gain compensation. Frames were saved at 2 Hz for 300 s. At 10 s, animals received a 750- to 1000-μL bolus injection of OMBs at a concentration of 1.0×10^9 OMBs/mL (gas volume fraction 50%) injected over 30 s. Following contrast elimination, animals were removed from anesthesia and allowed to recover before being returned to their cages.

DICOM CPS images were converted to AVI format and processed in Fiji software [26] to obtain time–intensity curves (TICs) for evaluation of microbubble circulation and elimination kinetics, calculated as pixel intensity arbitrary units (AU). Because of the high dose delivered, acoustic shadowing was observed in some of the animals. To minimize processing artifacts caused by acoustic shadowing, a region of interest (ROI) was selected by defining a 60- × 30-pixel oval over the peripheral region of the kidney proximal to the transducer rather than the entire kidney [25,27]. The average pixel intensity value of the ROI was determined for each frame and plotted over time to construct TICs. Data are presented as the mean ± standard deviation unless otherwise stated. All statistical analyses were performed in GraphPad Prism 9.4 (GraphPad Software, Inc., La Jolla, CA, USA). Values of $p < 0.05$ were considered to indicate statistical significance. Mean area under the curve (AUC) was calculated with an offset value of 20 and compared between the two groups via an unpaired *t*-test using the total area, standard error and total degrees of freedom of each group, similar to methods described previously [22]. Non-linear regression analysis was used to calculate the average elimination rate constant (K_e), half-lives and the standard error of the mean (SEM) of each group. Elimination rates, as well as half-life constants between the oxygen and air anesthesia groups, were compared via extra sum-of-squares *F*-test. Maximum intensity projection (MIP) images were produced by combining the maximum pixel values over time for each image in the series as a representative visualization of kidney perfusion in Fiji software [26].

Gas diffusion modeling

To investigate the microbubble dissolution during normal, oxygen and air breathing, we used the multigas microbubble dissolution model previously developed by Kwan and Borden [28,29]. The model predicts the size and gas content evolution by diffusion as a function of the microbubble shell properties and gas-environment composition using the expressions

$$\frac{dn_i}{dt} = \frac{4\pi R K_{H,i}}{\Omega_{s,i} + \Omega_{w,i}} \left(P_H + P_E - \frac{3BT}{4\pi R^3} \sum_j^N n_j - f_i P_{\infty,i} \right) \text{ where } i \neq j \quad (1)$$

$$0 = 2\sigma R^2 + P_H R^3 - \frac{4\pi}{3BT} \sum n_i \quad (2)$$

where n is the moles of gas in the microbubble core, i represents the gas species, t is the time coordinate, R is the radius of the microbubble, K_H is the molar Henry's constant, $\Omega_{s,i}$ is the dependence of gas permeation resistance through the lipid shell, $\Omega_{w,i}$ is the resistance of gas diffusion through the surrounding media, P_H is the hydrostatic pressure, P_E is the pressure exerted by the interface on the gas core, B is the ideal gas constant, T is the absolute temperature of the system and σ is the surface tension (also dependent on the shell and bubble radius, see below). The saturation fraction, f, relates the bulk partial pressure with the dissolved

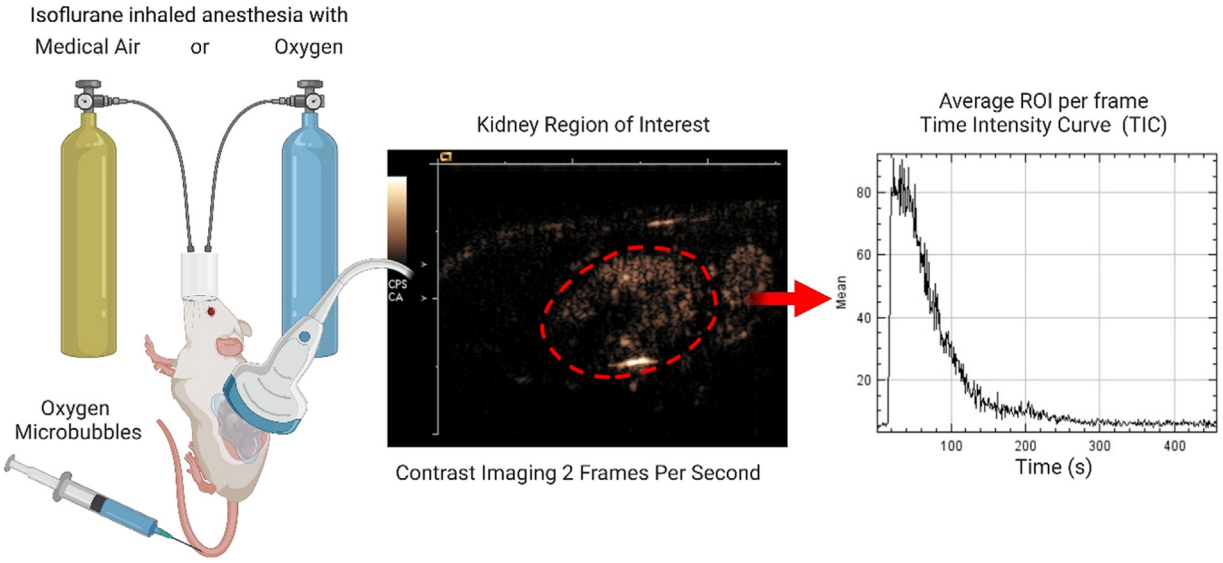

Figure 1. Schematic of experiment. Isoflurane, carried on medical air or pure oxygen, was used to anesthetize rats. Oxygen microbubbles were administered via intravenous bolus injection as contrast-specific ultrasound images of the kidney were acquired. Average contrast enhancement was calculated in a region of interest (ROI) per frame and plotted to build time–intensity curves from which area under the curve, a first-order exponential decay fit and half-lives were calculated.

gas saturation pressure P_∞. To estimate the dependence of gas permeation on the state of lipid encapsulation, the energy barrier model is implemented, as

$$\Omega_{s,i} = \Omega_n e^{\frac{\pi a_i^2}{k_B T}\Pi(R)} \quad (3)$$

where Ω_n is a constant dependent on the lipid shell composition, k_B is Boltzmann's constant, a is the collision radius for gas species i and $\Pi(R)$ is the surface pressure of the lipid shell ($\Pi(R) = \sigma(R) - \sigma_0$, where σ_0 is the surface tension of a free gas/water interface ~73 mN/m).

The surface tension during growth and microbubble compression is given by

$$\sigma = \begin{cases} 0 & \text{Resting} \\ \sigma_{EQ} + \left(\sigma_{break} - \sigma_{EQ}\right)e^{-K_E t} & \text{Expansion} \\ \sigma_{\beta_{max}} + k_c(\beta - \beta_{max}) & \text{Compression} \end{cases} \quad \ldots (4)$$

where k_E is the expansion modulus of the shell, σ_{EQ} is the equilibrium surface tension of the monolayer (25 mN/m), σ_{break} is the break-up tension, K_E is the relaxation rate, $\sigma_{\beta_{max}}$ is the tension of the monolayer at maximum strain (β_{max}) and k_c is the compression modulus. The DBPC shell and gas parameters are summarized in Tables S1 and S2 (online only). Mean partial pressures for dissolved O_2 in arterial blood from animals anesthetized with oxygen and air are listed in Table S3 (online only).

Results

There were visible differences in circulation kinetics for OMBs as a function of anesthetic carrier gases. Kidney perfusion was observed with OMBs in pure oxygen and medical air-breathing animals (Fig. 2). However, animals anesthetized on air exhibited enhancement at the proximal surface of the kidney and a decrease in enhancement beneath, consistent with acoustic shadowing. After maximum contrast enhancement, a decrease to baseline was observed in both groups. Overall, time–intensity curve analysis revealed significant differences in OMB circulation persistence between the two anesthetic carrier gases. The area under the curve was significantly higher in animals breathing air (3503 ± 98 AU) than in those breathing oxygen (906.6 ± 79.1 AU) ($p < 0.0001$). Contrast enhancement was significantly longer for animals breathing air than oxygen (Fig. 3). The average circulation half-lives for OMBs were 14.47 ± 0.21 and 5.48 ± 0.15 s ($p < 0.0001$) in animals breathing air and oxygen, respectively (Fig. 4).

Areas under the time–intensity curves for animals breathing air (3503 ± 98 AU) were statistically significantly greater compared with those for animals breathing oxygen (906.6 ± 79.1 AU) ($p < 0.0001$). The average half-life, calculated from a least-squares fit of a one-phase exponential decay of the time–intensity curves, was significantly longer for oxygen-breathing than for air-breathing animals (14.47 ± 0.21 and 5.48 ± 0.15 s, respectively; $p < 0.0001$, n = 6 per group).

To confirm our *in vivo* experimental results, we simulated microbubble dissolution by numerically solving eqns (1) and (2) using a first-order finite differences method in MATLAB (The MathWorks, Natick, MA, USA), as described previously [28,29]. The simulations predicted the dynamics of a 5.9 μm diameter microbubble initially filled with pure O_2 and suddenly immersed in arterial blood for an animal breathing either air or pure O_2. Partial pressures of O_2 and arterial blood pressure values were taken from Table S3 to compare the microbubble

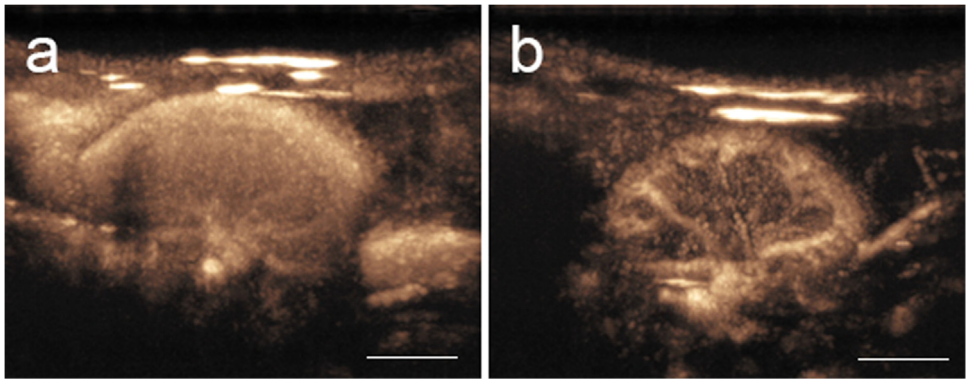

Figure 2. Representative maximum intensity projections of time series contrast ultrasound following oxygen microbubble intravenous injection when the animal is breathing air (a) or oxygen (b). Scale bar = 5 mm. Air-breathing animals exhibited more uniform perfusion compared with animals breathing oxygen, which exhibited enhancement mostly in larger vessels.

dissolution during air and oxygen breathing (Fig. 5). Figure 5A illustrates that breathing oxygen accelerates the microbubble dissolution rate (5.5 s), whereas breathing air increased the microbubble stability 6.3-fold versus oxygen breathing (35 s). Figure 5B illustrates that the O_2 content in the microbubbles quickly diffuses during O_2 breathing, while the presence of N_2 reduces the rate of O_2 efflux.

Discussion

Air-breathing animals exhibited substantial contrast enhancement, whereas oxygen-breathing animals exhibited incomplete perfusion of the kidney, likely because of dissolution of the OMBs before perfusion of the smaller vasculature. On maximum intensity projection, animals breathing air displayed even and complete perfusion, whereas oxygen breathing resulted in substantial enhancement in large vessels. Conversely to our initial hypothesis, we found that the contrast longevity of oxygen microbubbles injected into air-breathing animals was significantly longer than that of animals breathing oxygen. Recent contrast-enhanced ultrasound (CEUS) imaging protocols advocate intermittent imaging to reduce artificial depletion of contrast [30]. In our experiments, images were continuously acquired. Because of the low mechanical index and high perfusion in the kidney, it is unlikely that continuous imaging dramatically affected contrast longevity. In either case, both groups were imaged with the same parameters and would be similarly affected, allowing relativistic comparison. The bolus injection was administered by hand, using a timer for consistency. Future studies could employ a syringe pump to reduce variability. Beyond these minor experimental limitations, many potential factors may be responsible for the differences in contrast longevity observed.

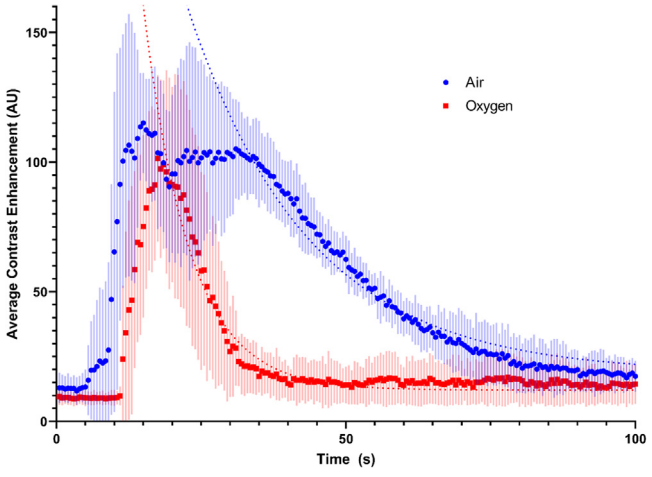

Figure 3. Time–intensity curves obtained from contrast-specific imaging. *Shaded area* represents standard deviation with the average drawn through each shaded region (n = 6 per group).

It has been determined that bolus injections of oxygen microbubbles may cause hemodynamic changes. When a very high dose of 1,2-distearoyl-*sn*-glycero-3-phosphatidylcholine (DSPC)/cholesterol bubbles were administered to rats, a significant reduction in mean arterial pressure (MAP) was observed along with an increase in pulmonary resistance [31]. Black et al. hypothesized that this was related to temporary pulmonary obstruction by the rather large bolus, compared with our studies. The current study was limited by the lack of advanced physiological monitoring, but animals breathing either gas received the same microbubble preparation. The relatively low-dose injections were well tolerated in both groups.

Choice of anesthetic carrier gas can affect systemic vascular tone. For example, breathing 100% oxygen led to a 20% reduction in cerebral blood flow in humans as measured by magnetic resonance imaging [32]. In rats, compared with air breathing, oxygen breathing resulted in lower respiration rates and increased mean arterial pressure [33]. Although both groups exhibited ventilation–perfusion mismatch, it was greater in animals breathing 100% oxygen. It has previously been determined that the anesthetic carrier gas has a significant effect on microbubble dissolution and circulation kinetics for air-filled protein-shelled microbubbles [34,35] and lipid-shelled perfluorocarbon microbubbles [36,37]. In their evaluation, Mullin et al. [36] found that, with the exception of pO_2 and pN_2, there was little difference in blood gas values between carrier gases, and they also suggested that respiration rate, heart rate and body temperature did not contribute to differences in circulation times [36]. They instead determined that for perfluorocarbon bubbles, the increase in contrast longevity when breathing air can be explained as a counterdiffusion of dissolved nitrogen into the bubble. The influx of N_2 into the bubble dilutes the O_2 already there, thereby reducing the pO_2 and the corresponding driving force for dissolution. Simulating injection of perfluorocarbon bubbles into arterial blood where the animal was breathing oxygen demonstrated a counterdiffusion of oxygen into the bubble, but because of oxygen's relatively high solubility in blood, the bubble dissolved more rapidly [36]. While breathing 100% oxygen, bubble and blood pO_2 differences in the arterial blood would be relatively small; however, in the venous blood pO_2 is only slightly elevated above normal [38], resulting in a large bubble–blood pO_2 gradient. Our results in this study reveal an effect similar to the findings of Mullin et al. [36], even with substantially increased oxygen delivery.

Because of increased contrast longevity, air is the recommended carrier gas for contrast ultrasound imaging experiments conducted under isoflurane anesthesia [39]. Compared with commonly used injectable

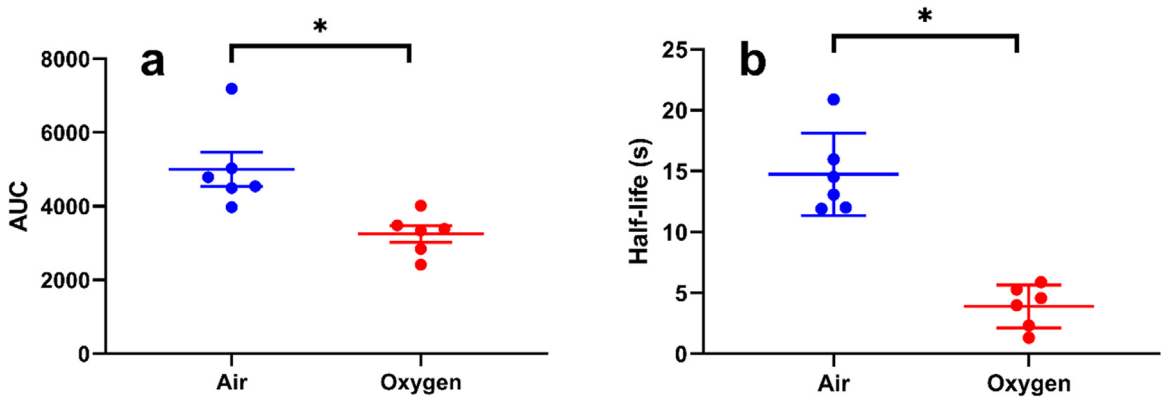

Figure 4. Area under the curve (AUC) (a) and half-life (b) analysis of the time–intensity curves for the air- and oxygen-breathing groups, revealing a significant difference in AUC ($p < 0.0001$) and half-life ($p < 0.0001$) between the two groups. Error bars represent standard error. n = 6 per group.

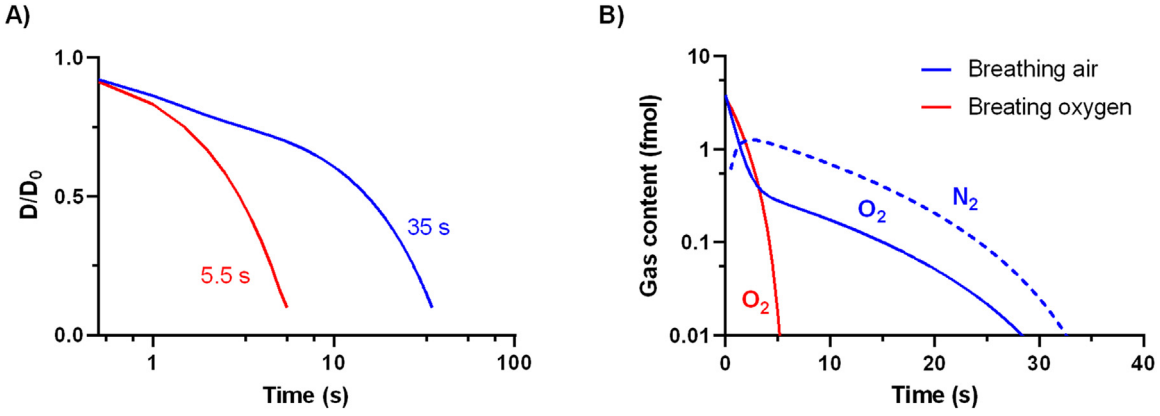

Figure 5. Gas diffusion modeling results for oxygen microbubbles injected intravenously into animals breathing medical air or pure oxygen. (A) Change in initial diameter over time for 5.9-μm simulated bubble. (B) Evolution of gas content over time for simulated microbubbles.

anesthetics, isoflurane is a respiratory depressant [40]. However, animals anesthetized via injectables are often spontaneously breathing air, which would likely have a similar effect on contrast longevity as breathing air under isoflurane anesthesia because of the nitrogen exchange occurring in the blood. Although our modeling data suggest this to be plausible, anesthetics vary in their cardiac, respiratory and hemodynamic impacts on the animal. Further studies directly comparing inhalational and injectable anesthetics would be useful to determine this definitively.

Other research exploring polymer-shelled oxygen microbubbles also reveal visibility on contrast ultrasound [19,20]. Their OMBs demonstrated contrast enhancement; however, contrast longevity was not explicitly reported *in vivo*. Over the two studies, the researchers did use both isoflurane and injectable anesthetics, but the study was not designed to allow direct comparison between the two. Modeling data suggest increased circulation persistence of OMBs on air is due to gas counterdiffusion between the bubble and the plasma. The increased lipid chain length reduces dissolution rate sufficiently to allow for nitrogen influx when breathing air, whereas in the oxygen case, the bubbles dissolve completely because of oxygen's solubility in blood and diffusion out of the bubble while in the venous circulation.

Conclusion

Lipid-shelled oxygen microbubbles formulated with DBPC persist in circulation longer when the animal is breathing medical air than when breathing pure oxygen under isoflurane anesthesia. This likely results from nitrogen counterdiffusion from plasma and tissue into the bubble as suggested by our modeling results. Therefore, contrast longevity in circulation as measured by contrast-specific ultrasound may not correspond directly to oxygen circulation kinetics as the bubble gas content changes over time.

Acknowledgments

This work was funded by National Institutes of Health grant R01CA232148. The funder had no role in study design, data collection, data analysis, data interpretation, writing of the article or decision to submit the article for publication.

Conflict of interest

P.G.D., M.B., P.A.D. and V.P. are all inventors or co-inventors on patents related to oxygen microbubble formulation and/or use. M.B. is also a founder and the chief scientific officer of Respirogen Inc. (Boulder, CO, USA). The other authors declare no competing interests.

Data availability statement

Data are available on reasonable request from the corresponding author.

Supplementary materials

Supplementary material associated with this article can be found in the online version at doi:10.1016/j.ultrasmedbio.2023.04.016.

References

[1] Quintiliani M. The oxygen effect in radiation inactivation of DNA and enzymes. Int J Radiat Biol Relat Stud Phys Chem Med 1986;50:573–94.
[2] Grimes DR, Partridge M. A mechanistic investigation of the oxygen fixation hypothesis and oxygen enhancement ratio. Biomed Phys Eng Express 2015;1:045209.
[3] Liu C, Lin Q, Yun Z. Cellular and molecular mechanisms underlying oxygen-dependent radiosensitivity. Radiat Res 2015;183:487.
[4] Ward JF. DNA damage produced by ionizing radiation in mammalian cells: identities, mechanisms of formation, and reparability. Prog Nucleic Acid Res Mol Biol 1988;35:95–125.
[5] Al Tameemi W, Dale TP, Al-Jumaily RMK, Forsyth NR. Hypoxia-modified cancer cell metabolism. Front Cell Dev Biol 2019;7:4.
[6] Shannon AM, Bouchier-Hayes DJ, Condron CM, Toomey D. Tumour hypoxia, chemotherapeutic resistance and hypoxia-related therapies. Cancer Treat Rev 2003;29:297–307.
[7] Colliez F, Gallez B, Jordan BF. Assessing tumor oxygenation for predicting outcome in radiation oncology: a review of studies correlating tumor hypoxic status and outcome in the preclinical and clinical settings. Front Oncol 2017;7:10.
[8] Elas M, Magwood JM, Butler B, Li C, Wardak R, DeVries R, et al. EPR oxygen images predict tumor control by a 50% tumor control radiation dose. Cancer Res 2013;73:5328–35.
[9] Gupta N, Saleem A, Kötz B, Osman S, Aboagye EO, Phillips R, et al. Carbogen and nicotinamide increase blood flow and 5-fluorouracil delivery but not 5-fluorouracil retention in colorectal cancer metastases in patients. Clin Cancer Res 2006;12:3115–23.
[10] Janssens GO, Rademakers SE, Terhaard CH, Doornaert P, Bijl H, van den Ende PVD, et al. Accelerated radiotherapy with carbogen and nicotinamide for laryngeal cancer: results of a phase III randomized trial. J Clin Oncol 2012;30:1777–83.
[11] Brown JM, Wilson WR. Exploiting tumour hypoxia in cancer treatment. Nat Rev Cancer 2004;4:437–47.
[12] Riess JG. Perfluorocarbon-based oxygen delivery. Artif Cells Blood Substit Immobil Biotechnol 2006;34:567–80.
[13] Xiang Y, Bernards N, Hoang B, Zheng J, Matsuura N. Perfluorocarbon nanodroplets can reoxygenate hypoxic tumors in vivo without carbogen breathing. Nanotheranostics 2019;3:135–44.
[14] Qin S, Caskey CF, Ferrara KW. Ultrasound contrast microbubbles in imaging and therapy: physical principles and engineering. Phys Med Biol 2009;54:R27–57.
[15] Fix SM, Borden MA, Dayton PA. Therapeutic gas delivery via microbubbles and liposomes. J Control Release 2015;209:139–49.
[16] Kwan JJ, Kaya M, Borden MA, Dayton PA. Theranostic oxygen delivery using ultrasound and microbubbles. Theranostics 2012;2:1174–84.
[17] Legband ND, Feshitan JA, Borden MA, Terry BS. Evaluation of peritoneal microbubble oxygenation therapy in a rabbit model of hypoxemia. IEEE Trans Biomed Eng 2015;62:1376–82.
[18] Fiala A, Slagle C, Legband N, Aghabaglou F, Buesing K, Borden M, et al. Treatment of a rat model of LPS-Induced ARDS via peritoneal perfusion of oxygen microbubbles. J Surg Res 2020;246:450–6.
[19] Eisenbrey JR, Shraim R, Liu JB, Li J, Stanczak M, Oeffinger B, et al. Sensitization of hypoxic tumors to radiation therapy using ultrasound-sensitive oxygen microbubbles. Int J Radiat Oncol Biol Phys 2018;101:88–96.
[20] Eisenbrey JR, Albala L, Kramer MR, Daroshefski N, Brown D, Liu JB, et al. Development of an ultrasound sensitive oxygen carrier for oxygen delivery to hypoxic tissue. Int J Pharm 2015;478:361–7.
[21] Fix SM, Papadopoulou V, Velds H, Kasoji SK, Rivera JN, Borden MA, et al. Oxygen microbubbles improve radiotherapy tumor control in a rat fibrosarcoma model—a preliminary study. PLoS One 2018;13:e0195667.
[22] Reusser TD, Song KH, Ramirez D, Benninger RK, Papadopoulou V, Borden MA. Phospholipid oxygen microbubbles for image-guided therapy. Nanotheranostics 2020;4:83–90.
[23] Peng S, Song R, Lin Q, Zhang Y, Yang Y, Luo M, et al. A robust oxygen microbubble radiosensitizer for iodine-125 brachytherapy. Adv Sci (Weinh) 2021;8:2002567.
[24] McEwan C, Owen J, Stride E, Fowley C, Nesbitt H, Cochrane D, et al. Oxygen carrying microbubbles for enhanced sonodynamic therapy of hypoxic tumours. J Control Release 2015;203:51–6.
[25] Fix SM, Nyankima AG, McSweeney MD, Tsuruta JK, Lai SK, Dayton PA. Accelerated clearance of ultrasound contrast agents containing polyethylene glycol is associated with the generation of anti-polyethylene glycol antibodies. Ultrasound Med Biol 2018;44:1266–80.
[26] Schindelin J, Arganda-Carreras I, Frise E, Kaynig V, Longair M, Pietzsch T, et al. Fiji: an open-source platform for biological-image analysis. Nat Methods 2012;9:676–82.
[27] Chen CC, Sirsi SR, Homma S, Borden MA. Effect of surface architecture on in vivo ultrasound contrast persistence of targeted size-selected microbubbles. Ultrasound Med Biol 2012;38:492–503.
[28] Kwan JJ, Borden MA. Lipid monolayer dilatational mechanics during microbubble gas exchange. Soft Matter 2012;8:4756–66.
[29] Kwan JJ, Borden MA. Microbubble dissolution in a multigas environment. Langmuir 2010;26:6542–8.
[30] Wilson SR, Lyshchik A, Piscaglia F, Cosgrove D, Jang HJ, Sirlin C, et al. CEUS LI-RADS: algorithm, implementation, and key differences from CT/MRI. Abdom Radiol 2018;43:127–42.
[31] Black KJ, Lock AT, Thomson LM, Cole AR, Tang X, Polizzotti BD, et al. Hemodynamic effects of lipid-based oxygen microbubbles via rapid intravenous injection in rodents. Pharm Res 2017;34:2156–62.
[32] Watson NA, Beards SC, Altaf N, Kassner A, Jackson A. The effect of hyperoxia on cerebral blood flow: a study in healthy volunteers using magnetic resonance phase-contrast angiography. Eur J Anaesthesiol 2000;17:152–9.
[33] Wilding LA, Hampel JA, Khoury BM, Kang S, Machado-Aranda D, Raghavendran K, et al. Benefits of 21% oxygen compared with 100% oxygen for delivery of isoflurane to mice (*Mus musculus*) and rats (*Rattus norvegicus*). J Am Assoc Lab Anim Sci 2017;56:148–54.
[34] Wible JH, Wojdyla JK, Bales GL, McMullen WN, Geiser EA, Buss DD. Inhaled gases affect the ultrasound contrast produced by Albunex in anesthetized dogs. J Am Soc Echocardiogr 1996;9:442–51.
[35] Wible Jr J, Wojdyla J, Bugaj J, Brandenburger G. Effects of inhaled gases on the ultrasound contrast produced by microspheres containing air or perfluoropropane in anesthetized dogs. Invest Radiol 1998;33:871–9.
[36] Mullin L, Gessner R, Kwan J, Kaya M, Borden MA, Dayton PA. Effect of anesthesia carrier gas on in vivo circulation times of ultrasound microbubble contrast agents in rats. Contrast Media Mol Imaging 2011;6:126–31.
[37] Itani M, Mattrey RF. The effect of inhaled gases on ultrasound contrast agent longevity in vivo. Mol Imaging Biol 2012;14:40–6.
[38] Whalen RE, Saltzman HA, Holloway Jr DH, McIntosh HD, Sieker HO, Brown Jr. IW. Cardiovascular and blood gas responses to hyperbaric oxygenation. Am J Cardiol 1965;15:638–46.
[39] Hyvelin JM, Tardy I, Arbogast C, Costa M, Emmel P, Helbert A, et al. Use of ultrasound contrast agent microbubbles in preclinical research: recommendations for small animal imaging. Invest Radiol 2013;48:570–83.
[40] Tsukamoto A, Serizawa K, Sato R, Yamazaki J, Inomata T. Vital signs monitoring during injectable and inhalant anesthesia in mice. Exp Anim 2015;64:57–64.